Available online at www.sciencedirect.com
SCIENCE DIRECT®
ELSEVIER
Deep-Sea Research I 52 (2005) 1789–1805
DEEP-SEA RESEARCH PART I
www.elsevier.com/locate/dsr

Inter-annual variability in the thermal structure of an oceanic time series station off Ecuador (1990–2003) associated with El Niño events

José Garcés-Vargas[a,b,*], Wolfgang Schneider[a,b], Rodrigo Abarca del Río[b,c], Rodney Martínez[d,1], Eduardo Zambrano[d]

[a] *Universidad de Concepción, Facultad de Ciencias Naturales y Oceanográficas, Departamento de Oceanografía, Programa de Doctorado en Oceanografía, Cabina 5, Casilla 160-C, Concepción, Chile*
[b] *Universidad de Concepción, Centro de Investigación Oceanográfica en el Pacífico Sur-Oriental (COPAS), Casilla 160-C, Concepción, Chile*
[c] *Universidad de Concepción, Facultad de Ciencias Físicas y Matemáticas, Departamento de Geofísica, Casilla 160-C, Concepción, Chile*
[d] *Instituto Oceanográfico de la Armada (INOCAR), Departamento de Oceanografía y Clima, División de Oceanografía Física, Avenida 25 de Julio—vía Puerto Marítimo, Casilla 5940, Guayaquil, Ecuador*

Received 31 December 2003; received in revised form 20 August 2004; accepted 25 May 2005
Available online 3 August 2005

Abstract

Previously unpublished data (1990–2003) from a marine station located 20 km off the coast of Ecuador (Station La Libertad, 02°12′S, 080°55′W) are employed to investigate oceanic inter-annual variability in the far eastern equatorial Pacific, and its relation to the central-eastern equatorial Pacific. La Libertad is the only time series station between the Galapagos Islands and the South American coast, the region most affected by El Niño events (El Niño 2 region, 0–5°S, 90°W–80°W). Although configured and serviced differently, station La Libertad can be looked at as an eastern extension of the TAO/TRITON monitoring system, whose easternmost mooring is located at 95°W, 1550 km offshore. This study of El Niño's impact on the thermocline and its relationship to sea surface temperature revealed anomalies in the thermocline at station La Libertad some 2–4 months before their appearance at the sea surface. Inter-annual variability, namely quasi-biennial and quasi-quadrennial oscillations, accounts for roughly 80% of the total variance in temperature anomalies observed in the water column at station La Libertad.

The coincidence in both phase and amplitude of these inter-annual oscillations explains the strength of El Niño events in the water column off La Libertad. We further show that anomalies in heat content appear 8–9 weeks earlier at

*Corresponding author. Universidad de Concepción, Facultad de Ciencias Naturales y Oceanográficas, Departamento de Oceanografía, Programa de Doctorado en Oceanografía, Cabina 5, Casilla 160-C, Concepción, Chile. Tel.: +56 41 203493; fax: +56 41 256571.
E-mail address: jgarces@udec.cl (J. Garcés-Vargas).
[1]Present address: Centro Internacional para la Investigación del Fenómeno de El Niño (CIIFEN), Escobedo y 9 de Octubre 1204, Guayaquil, Ecuador.

doi:10.1016/j.dsr.2005.05.008

140°W in the equatorial Pacific (6550 km away from the coast) than at the coast itself. The arrival of El Niño, which has important regional social consequences as well as those for local fisheries, could therefore be predicted in the sub-surface waters off Ecuador by using these anomalies as a complementary index. In addition, the speed of the eastward propagation of these El Niño-associated anomalies' suggests the possible participation of higher-order baroclinic mode Kelvin waves and associated interaction processes in the eastern Pacific, which should be further investigated.

Keywords: El Niño; Quasi-biennial and quasi-quadrennial oscillations; Heat content; Eastern equatorial Pacific; Ecuador; La Libertad

1. Introduction

The inter-annual variability of sea surface temperature (SST) in the tropical Pacific Ocean is dominated by the El Niño-Southern Oscillation (ENSO) (e.g. Cane, 1983; Rasmusson and Wallace, 1983), one of the most important ocean-atmosphere interactions. Kelvin waves originate in the warm pool of the western equatorial Pacific, then travel along the equatorial Pacific and manifest themselves as anomalous warm events off the South American coast (Boulanger and Fu, 1996; McPhaden and Yu, 1999). These events are known as ''El Niño''. Off the coast of Ecuador, SST rises a few degrees Celsius above normal; during the 1982/1983 El Niño event, the thermocline deepened more than 80 m (Cucalón, 1987). Extremely high temperatures affect the local economy by causing mortality in fish and birds (Barber and Chavez, 1983), as well as exercising a strong influence over the climatological oceanic heat balance off Ecuador and Peru.

Owing to its importance, the evolution of El Niño events and their possible relation to large-scale oscillations have been studied by numerous authors. Zhang et al. (1998) analyzed 43 years of monthly averaged SST in the Pacific between 58°N and 20°S, with respect to low-frequency components, based on 4° latitude by 8° longitude averages. The authors found three dominant modes: inter-decadal, quasi-quadrennial (QQ), and quasi-biennial (QB). The latter two modes were largest in the Tropics and are interpreted to be two distinctive ENSO modes. Similar results were presented by Jiang et al. (1995) in a study of the same SST data base (between 4°N and 4°S) and regional zonal sea surface winds. In their study, the QQ mode dominated the variance and had the most distinct and energetic spectral peak. Brassington (1997) also showed significant energy in the QQ and QB period modes for the Southern Oscillation Index (SOI) alone from 1876 to 1995. Decadal, inter-annual, and QB signals were also found by White et al. (2003), who used an extended Empirical Orthogonal Function approach to analyze 45 years of data (1955–2000) from the Pacific Ocean between 30°S and 30°N as to SST, the depth of the 18 °C isotherm, zonal and meridional sea surface winds, and wind stress curl. A slowly eastward-propagating, warm SST anomaly was found in each signal. Using TAO/TRITON mooring data, McPhaden (1999) presented the eastward propagation of heat content anomalies within the first 400 m of the water column from the western equatorial Pacific, along the Equator, to 95°W in the evolution of the 1997/1998 El Niño. Meinen and McPhaden (2000) showed that warm water volume anomalies, integrated above the depth of the 20 °C isotherm between 5°N and 5°S and 120°E and 80°W using the Neville Smith gridded sub-surface data set, led Niño 3 SST anomalies by 7 months.

These results depict well the imprint of the ENSO phenomena on SST and sub-surface temperatures over most of the Pacific basin. Nevertheless, there are only a few studies on more local processes and their interactions with large-scale variability. East of the Galapagos Islands (Niño 2 region), scarce information exists about the temporal vertical thermal structure of the water column, and hence about the ENSO impact therein. Here, for the first time, we introduce and analyze oceanic data (1990–2003) from the station La Libertad, off Ecuador. La Libertad is the only time series station between the Galapagos Islands and the South American coast, which is the area most affected by El Niño. The location of station La Libertad, approximately 2°S, allows the monitoring of guided Kelvin waves as well as contributions of Rossby waves and other processes.

This paper analyzes temperature anomalies throughout the water column in order to better understand the inter-annual variability of the thermal structure of the water column off Ecuador associated with El Niño events. The relationship between these anomalies and equatorial Pacific variability is investigated. The time dependency between thermocline anomalies and SST anomalies is also determined.

2. Data and methodology

The time series station, La Libertad (02°12′S, 080°55′W), is situated 20 km offshore from the city of La Libertad, Ecuador, and is maintained by the Instituto Oceanográfico de la Armada (INOCAR), Ecuador. The station has been occupied since May 1990, and this study analyzes data compiled from the initiation of the time series to May 2003 (Fig. 2c includes data up to November 2003). Water depth at the station is about 100 m, the sampling interval is about 2–3 weeks, and the vertical resolution is 1 m. Data are collected with a Sea-Bird 19 CTD. Temperature time series were computed on a fortnightly resolution by linear interpolation at each depth increment. In order to eliminate spiky erroneous data, a central moving average filter, including 2 intervals on each side of the central point, was applied to the time series, which corresponds to a filtered window of $2\frac{1}{2}$ months. A time series of the 20 °C isotherm depth was also computed as a proxy for the depths of the base of the thermocline. Daily average sea level data from the tide gauge located in La Libertad harbor operated by INOCAR, 20 km from the time series station (January 1975–May 2003) are also used here. Time series anomalies were calculated by subtracting the average annual cycle computed over the whole period. We complemented our data set with temperature data (May 1990–May 2003) and their anomalies from the TAO/TRITON moorings (McPhaden et al., 1998) at 110°W, 140°W, 170°W, and 165°E along the equatorial Pacific, averaged between 2°N and 2°S.

Spectral analysis (Fourier transform) and wavelet technique is employed in a comparative way to assess the behavior of the time series anomalies in time. Conventional Fourier analysis allows determining which frequencies appear in the signal as a whole (Fig. 3), but fails to efficiently reveal the time dependence of these spectral features.

Instead the basic goal of wavelet analysis is to both determine the frequency content of a time series, and assess how this frequency content changes in time. A wavelet transform represents the function as a sum of time-shifted (translated) and scaled (dilated) representations of some arbitrary function, which is called a wavelet. By examining the time series on all scales wavelet transform naturally separates the existing oscillations within the original signal and allows the observation of amplitude modulations within frequency domains.

To analyze the data sets we chose wavelet multi-resolution analysis via Daubechies' discrete wavelet transform (DWT, Daubechies, 1992; Mallat, 1998). This technique has been used, for example in meteorology analyzing time series of precipitation (Kumar and Foufoula-Georgiou, 1997), and in oceanography examining time series of sub-tidal fluctuations (Percival and Mofjeld, 1997). Wavelet multi-resolution analysis is among one of the main applications of DWT. A description of this technique is outlined in Appendix A.

By forming a series of half-band filters that divide a spectrum into a high-frequency and a low-frequency band, the original signal is decomposed into a hierarchical set of j approximations (low frequencies) and j details (high-frequencies). We chose 7 levels of decomposition considering the length of the time series and because fewer levels did not allow the separation of different annual time scales. This decomposition resulted in 7 details (D1–D7, from high to low frequencies) and one approximation (A7), which represents the low frequency oscillations not captured within the details.

Particular care was taken to test the usefulness and significance of this method for this relatively short time series (in the sense that only 3 moderate or strong El Niño events are covered), by analyzing longer time series of tide gauge measurements taken close by and then comparing results from the long record and overlapping periods (see below).

3. Time series station La Libertad

3.1. Temperature anomalies and their relationship with El Niño events

Total temperature and temperature anomalies at station La Libertad are presented in Figs. 1b and d as functions of depth and time, respectively. The depth of the 20 °C isotherm is over plotted in both panels. SST and its anomalies are shown separately in Figs. 1a and c. Mixed layer temperatures vary between 20 and 26 °C, whereas the rest of the water column ranged between 15 and 20 °C. A seasonal SST cycle is evident (Fig. 1a), although the station's almost equatorial position had led us to expect a semi-annual cycle. Solar radiation at the outer atmosphere reaches its second annual maximum during the second half of the year. During this period, cloud cover, mainly low stratocumulus clouds, increases, thereby reducing heat flux into the ocean and depressing the

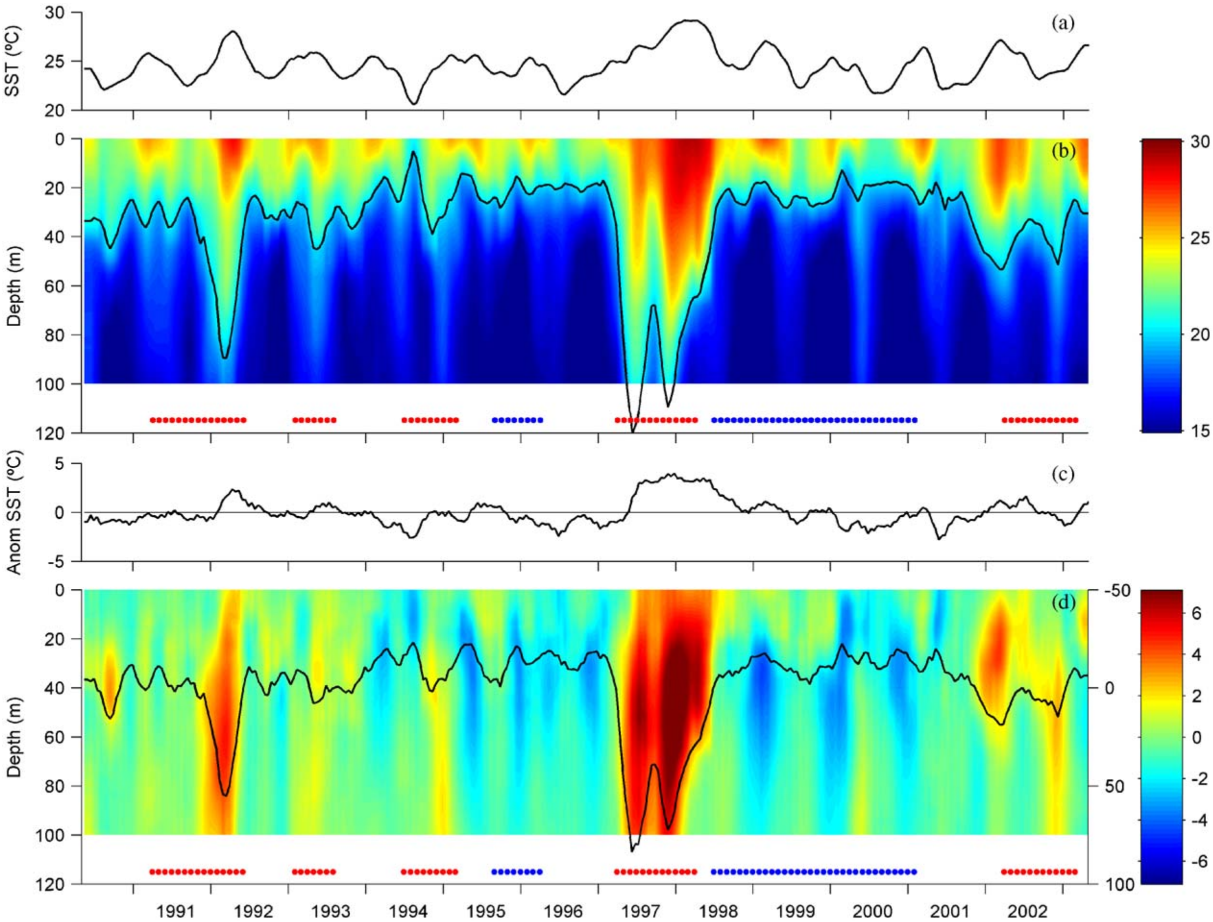

Fig. 1. Data and anomalies from time series station, La Libertad (May 1990–May 2003), from surface (0 m) to bottom (100 m), panels b) and d), respectively. El Niño (red dots) and La Niña (blue dots) phases are indicated according to El Niño 3.4 index. Units are in °C, the right hand vertical color bar applies. (a) Sea surface temperature; (b) Temperature and depth of the 20 °C isotherm (solid black line); (c) Sea surface temperature anomalies; (d) Temperature anomalies and 20 °C isotherm anomaly (solid black line, the right-hand side depth scale in *m* applies).

evolution of a semi-annual cycle (Köberle and Philander, 1994; meteorological observations by INOCAR, not shown here). Large positive SST anomalies at station La Libertad are strongly associated with recent moderate and strong El Niño events from 1991/1992, 1997/1998, and 2002/2003. The weak El Niño events from 1993 and 1994/1995 only show small positive SST anomalies and are not treated here (Fig. 1c). The depth of the 20 °C isotherm, which is relatively shallow (about 20 m) in non-El Niño episodes, descended all the way to the bottom at station La Libertad, hence exceeding more than 100 m depth during the 1997/1998 El Niño (linear extrapolation placed the 20 °C isotherm at about 120 m, as shown in Fig. 1b). The temperature anomalies within the thermocline nearly doubled the magnitude of those observed at the sea surface; maximum anomalies of 8 °C (thermocline) and 4 °C (sea surface) were observed during the 1997/1998 El Niño. In the following, we therefore investigate the relationship between the thermocline and SST anomalies during El Niño episodes.

SST anomalies and thermocline anomalies (the latter computed as depth-averaged temperature anomalies for the 20–80 m water column) were computed as depth-averaged temperature anomalies for the 20–80 m water column for the three El Niño events captured in the La Libertad time series (Figs. 2a–c). The anomalous warm moderate 1991/1992 El Niño episode started at the sea surface in February 1992 and lasted until September 1992. Anomalous warm SST increased up to 2.3 °C in April 1992. The main warming event had already started in the thermocline in October 1991 and lasted there until May 1992, with maximum depth-averaged temperature anomalies of 4.3 °C in March 1992. The 20 °C isotherm (Z20) descended a maximum of 55 m in February/March 1992 (Figs. 1b and d).

The strong 1997/1998 El Niño event arrived off Ecuador at the end of May 1997 (sea surface) and positive anomalies in SST were observed until November 1998. Maximum anomalies of 4.0 °C were recorded at the end of 1997, and anomalous high temperatures above 2.5 °C between July 1997 and June 1998 (Fig. 2b). In the thermocline, the onset of the warm event took place as early as

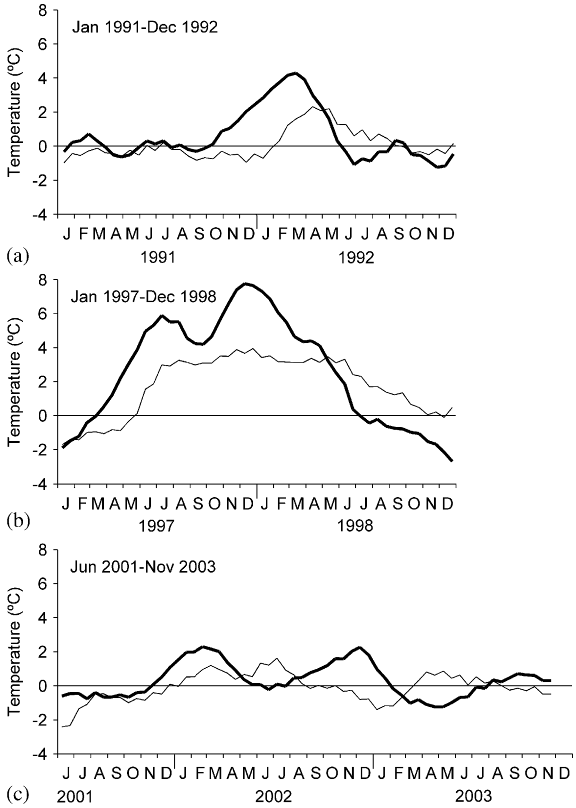

Fig. 2. Temperature anomalies for moderate and strong El Niño events at station La Libertad. Thick solid lines represent depth-averaged temperature anomalies (20–80 m, thermocline), and thin solid lines SST anomalies. (a) January 1991/December 1992; (b) January 1997/December 1998; (c) June 2001/November 2003.

March 1997. High depth-averaged temperature anomalies greater than 7.5 °C were reached between November 1997 and January 1998 and faded in June 1998. The motion of the Z20 is characterized by a double peak, moving downwards by 85 m in the middle of 1997 and 73 m in December 1997 (Figs. 1b and d). This double peak pattern is repeated in the depth-averaged temperature anomalies (Fig. 2b).

Two periods of positive SST anomalies (thin line in Fig. 2c) were noted during the moderate 2001/2003 El Niño events, namely, January–August 2002, and April–August 2003. The maximum anomalies reached about 1.6 °C in July 2002. Significant positive depth-averaged temperature anomalies, with a maximum of more than 2.0 °C, were already registered in the thermocline from December 2001 to May 2002 and from August 2002 to January 2003; in the latter period, SST showed a negative anomaly. The 20 °C isotherm only showed a modest drop of 15–20 m from its average position compared to the former two El Niño events; in 1997, it reached the bottom twice. Maximum temperature anomalies reached more than 4 °C at depths between 15 and 35 m in the beginning of 2002 and about 2.5 °C at depths between 35 and 60 m at the end of 2002 (Fig. 1d), again sharply exceeding SST anomalies. Since depth-averaged temperature anomalies were computed for the 20–80 m depth range, maximum temperature anomalies are not fully represented because of the Z20's relatively shallow depth.

Thus, the time lag between maximum temperature anomalies in the thermocline and at the surface is event-dependent, with changes in the thermocline always preceding those at sea surface by 2–4 months. For example, during the onset of El Niño 1991/1992, the thermocline led sea surface by roughly 4 months, whereas the lag was reduced to 2.5 months in 1997/1998. This difference was also seen at the event's termination; thermocline led surface by 3.5 months in 1991/1992 and by almost 5 months in 1997/1998. During the somewhat weaker 2002/2003 event, a phase lag between anomalies of depth-averaged temperature and SST was also evident. The onset of depth-averaged temperature anomalies led SST by 2 months at the end of 2001 and faded in May 2002 (Fig. 2c), 3 months earlier than SST. SST anomalies showed a weak cold phase during the second half of 2002, whereas depth-averaged temperature anomalies were positive again from August 2002 to January 2003, announcing the arrival of positive SST anomalies in March 2003. In this case, however, the phase lag was much longer. Negative depth-averaged temperature anomalies, (February 2003–June 2003) preceded negative SST anomalies, which were observed starting in September 2003.

Nevertheless, when considering the time lags between the appearance of anomalies within the thermocline and at the surface as observed in 1991/1992 and 1997/1998, maximum positive anomalies were noted in the thermocline in March 2002, 4 months before a maximum anomaly showed up at the surface. Again, at the end of December 2002, maximum positive anomalies were observed in the thermocline 5 months before the surface warmed up maximally in May 2003. A similar pattern was observed for the weak 1994/1995 event (Figs. 1c and d). Cross correlations between SST and thermocline anomalies at station La Libertad, considering the whole 13-year record, resulted in a highest correlation ($R = 0.73$) at a time lag of about 3.5 months. Taking into account the number of years analyzed (13), all correlations above $R = 0.62$ are significant at the 95% significance level (using a student's *t*-test), whereas correlations higher than $R = 0.52$ fall into the 90% significance band.

Positive SST anomalies at station La Libertad, varying in magnitude and duration, were associated with recent moderate and strong El Niño events from 1991/1992, 1997/1998, and 2002/2003. Positive temperature anomalies within the thermocline reached the coast of Ecuador earlier than the SST anomalies. Moreover, the magnitude of the thermocline anomalies was nearly double those observed at the surface.

3.2. Oscillations in temperature and sea level anomalies

A power spectrum computed for each time series of temperature anomalies (surface to 100 m depth) (Fig. 3) allowed us to investigate the frequencies present in the water column. Most of the power was concentrated at inter-annual time scales (1.3–7 years) at depths between 20 and 60 m. The highest amplitudes, concentrated at about 40 m depth, and were observed around periods of 3 and 5 years. The power observed on intra-seasonal frequencies (periods of about 9–10 month) was, interestingly, concentrated below the surface, between 15 and 80 m. However, its characteristics as well as its interaction with other frequencies via non-linear processes are part of another line of research that will be reported elsewhere. Energy at low-frequency time scales is less powerful and, due to the limited length of the time series, statistically insignificant. In contrast, previous works on the

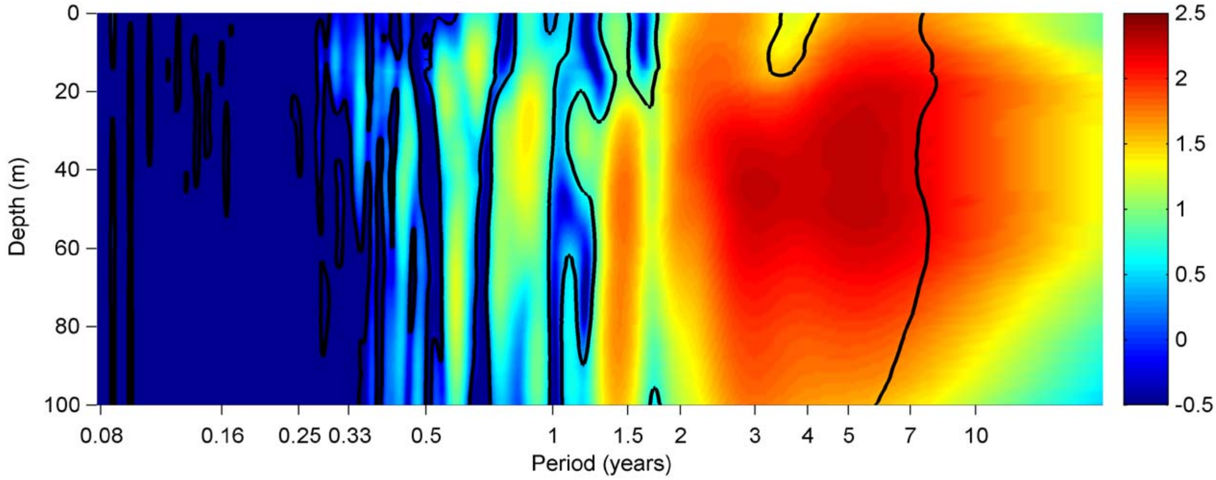

Fig. 3. Log 10 of power spectrum density from May 1990 to May 2003 for temperature anomalies from surface (0 m) to bottom (100 m) at station La Libertad. Units are $^{\circ}C^2$/cptw (cptw = cycles per 2 weeks), the right hand vertical color bar applies. Solid black line represents 95% significance level obtained from an autoregressive model of order 1.

tropical Pacific zone (Hasegawa and Hanawa, 2003a, b), have also revealed decadal time scales for thermal variability.

The inter-annual oscillations observed in the power spectra of our time series of temperature anomalies surpasses the 95% significance level, according to a red noise background spectrum. Below, we only discuss the analysis of the statistically-significant inter-annual peaks, leaving the weaker non-significant lower frequencies and the high frequency components for a later study.

Nevertheless, the presence of low-frequency fluctuations in our time series might influence the results obtained when analyzing the 13-year record. Moreover, the periods of inter-annual fluctuations examined in this study can only be interpreted based on the coarse resolution provided by spectral and wavelet analyses. We therefore attempted to show that the lower frequency contributions in our time series played only a minor role and that the inter-annual results obtained were consistent with longer time series.

To this end, we first analyzed the time series of mean sea level anomalies from La Libertad (Fig. 4a, thin line), extending over 28 years and including the period of our temperature data. In the same figure, anomalies of depth-averaged temperature of the whole water column, which can be related to anomalies of heat content of the whole water column via $h_c = \rho_o C_p \Delta T$ (where, h_c is the heat content, ρ_o, is the density of seawater, C_p, is the heat capacity, and ΔT is the anomaly of depth-averaged temperature), are shown for the overlapping period (thick line). Anomalies of depth-averaged temperature correlate very well with mean sea level anomalies within the overlapping period of 13 years ($R = 0.82$). Taking further into account that anomalies in mean sea level and upper water column temperature in the eastern equatorial Pacific are mainly caused by ENSO dynamics (Jin, 1997), and therefore generally correlate well (e.g. McPhaden and Yu, 1999), the results obtained by a wavelet decomposition of the long time series of mean sea level anomalies at La Libertad should resemble the results obtained when analyzing anomalies of depth-averaged temperatures from the same period.

We choose a 7-level wavelet decomposition since it separates well the different significant inter-annual signals from the lower frequencies, which are contained within the highest level, the A7 approximation. Detail levels D5, D6, and D7 represent inter-annual time scales associated with average periods of 2.1, 4.3, and 6.3 years,

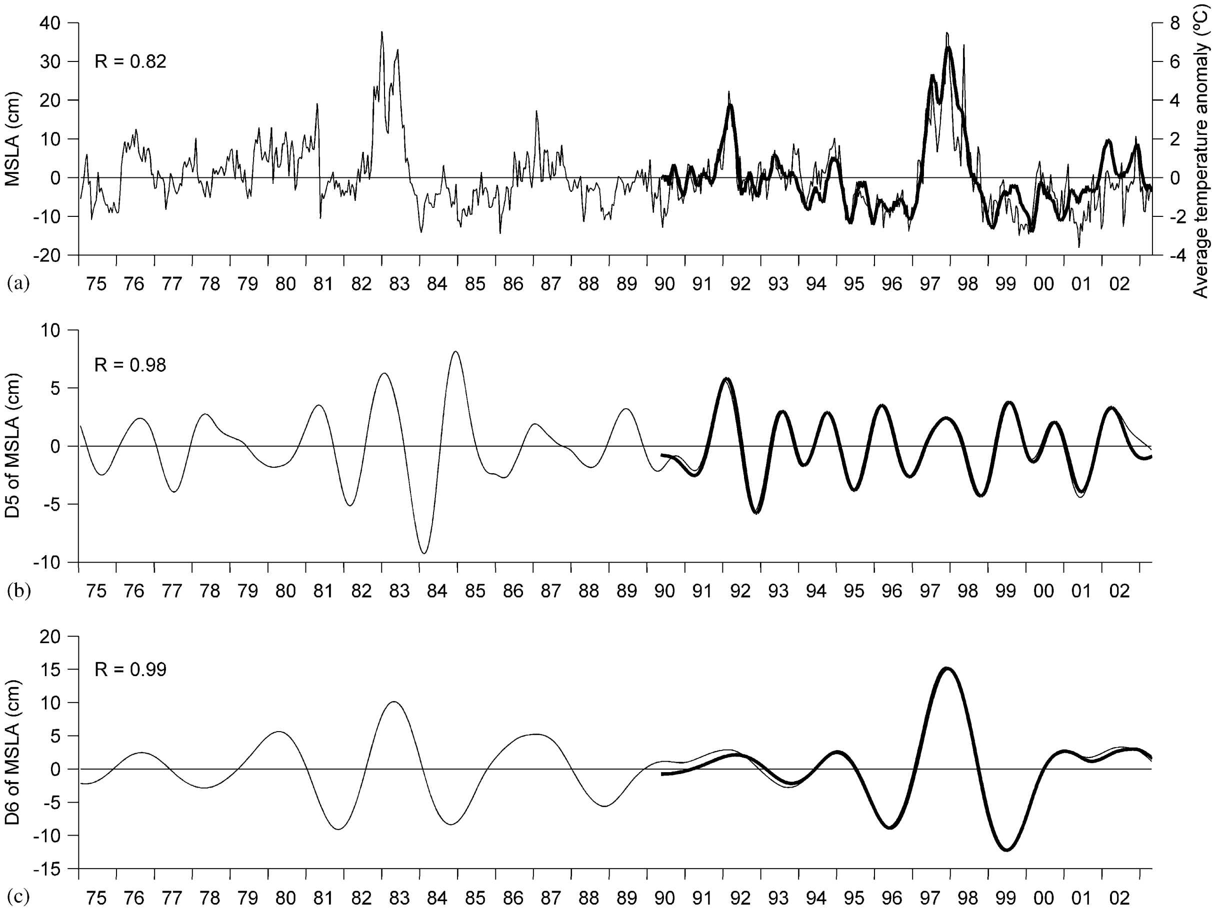

Fig. 4. (a) Mean sea level anomaly (thin solid line) and average temperature anomaly (thick solid line); (b) detail D5 (the spectral band covers roughly 1.5–2.7 years); and (c) detail D6 (the spectral band covers roughly 2.4–6.2 years; main energy was found between 3 and 4.5 years). In (b) and (c), the thin solid line represents the original time series (1975–2003) and the thick solid line represents the padded time series (1990–2003).

respectively (Table 1). The decomposition was computed for two time series of mean sea level anomalies at La Libertad, namely 1975–2003 and 1990–2003. The results of both analyses correlated remarkably well within their overlapping period, and Figs. 4b and c show the fifth (D5) and sixth details (D6) associated with QB (Correlation coefficient, $R = 0.98$) and QQ oscillations (Correlation coefficient, $R = 0.99$), respectively. We are, therefore, confident as to the robustness of the method used in this research of inter-annual time scales of temperature anomalies at station La Libertad between 1990 and 2003.

Moreover, the sum of the lower modes (A7 approximation) explained, on average, less than 9% of the variance in mean sea level anomalies, decreasing to roughly 6% when considering only 1990–2003. Longer time scales between 1975 and 2003 played a minor role in mean sea level variability and, by extension (to a first approximation), in the mean thermal structure.

Detail levels D5, D6, and D7 present inter-annual time scales that explain 8.2%, 37%, and 9.8% of the variance of the mean sea level anomalies from 1975–2003, whereas the percentages of the variance explained are changed to

Table 1
Wavelet analysis: station La Libertad

Detail	Temperature (0–100 m)		MSLA		Z20	
	Period (Years)	Variance (%)	Period (years)	Variance (%)	Period (years)	Variance (%)
A7		1.1		4.2		0.03
D7	6.4	7.4	6.3	12.9	6.6	8.7
D6	4.6 [2.5, 6.8]	49.9	4.3 [2.4, 6.2]	41.8	4.6 [2.6, 6.6]	48.8
D5	1.9 [1.3, 2.4]	21.2	2.1 [1.5, 2.7]	8.4	2.1 [1.3, 2.8]	25.2
D4	0.9	11.9	0.9	8.1	0.9	6.0
D3	0.6	7.2	0.5	12.5	0.7	10.4
D2	0.4	0.9	0.2	5.5	0.3	0.6
D1	<0.2	0.4	<0.2	6.5	<0.2	0.3

For each detail, the central period of its frequency band and the variance explained by each detail are listed. For Detail 5 and Detail 6 the upper and lower limits of the frequency band are also given in brackets. Depth-averaged temperature anomalies (Temperature, 0–100 m), mean sea level anomalies (MSLA), and the depth of the 20 °C isotherm (Z20). The central period, associated with the largest amplitude, and the band width, defined by half amplitude method, was referred from a harmonic analysis of each detail obtained.

8.4%, 41.8%, and 12.9% when computed solely for 1990–2003 (Table 1). The fourth detail (D4) is associated with an average period of 0.8 years and explains 8.1% of the total variance. The main peak within this detail occurred at a period of 0.9 years and was followed by a smaller peak at about 1.3 years. However, the contributions of inter-annual variability within this detail are minor, so detail D4 will not be taken into account in the following analyses. We relate the A7 approximation to low-frequency time scales that are not considered in this research. The details D5, D6, and D7 are related, respectively, to QB, triennial-quadrennial (QQ), and 5–6 year oscillations (FY).

3.3. Analysis of inter-annual modes in the water column

Encouraged by the dominance of the inter-annual modes in the anomalies of mean sea level, the above 7-level wavelet decomposition was also applied to the time series of temperature anomalies and to the Z20 anomalies from station La Libertad. Prior to running the routine, the 13 years of data were padded with zeroes. We applied the zero padding, first to reduce both side and end effects, and also to extend the length of the time series to match the length of the mean sea level record. The results are as follows (Table 1).

The QB mode (Fig. 5a) accounted for 21.2% and 25.2% of the temperature and Z20 anomalies, respectively, whereas the QQ mode alone (Fig. 5b) explained 49.9% and 48.8%, and the FY mode (Fig. 5c) roughly 8% in both. The sum of all three modes explained 78.6% and 82.0% of the variability of temperature and Z20 anomalies in the entire water column, whereas the sum of the first two modes explains the main variance (71.1% and 74.0%) (Fig. 5d). In the QQ mode, positive amplitudes were moderate in 1992, but very high between 1997/mid-1998, especially in the thermocline (20–80 m). The amplitudes were also reasonably elevated within 20–60 m of the water column in 2002 (Fig. 5b). The QB mode, on the other hand, presented more regular behavior: temperatures were elevated in the beginning of 1992, mid-1993 and 1997, the end of 1999, and in the upper meters as well in 2002. The coincidence of positive amplitudes in the QQ and QB modes gave rise to moderate and strong El Niño events in 1991/1992 and 1997/1998 (Fig. 5d), also depending on the magnitude of the amplitudes of both contributions. Interestingly, the phase of the FY mode, was associated with the peaks of these two events, although its amplitude is rather weak compared to the QB and QQ modes. The degree to which the depth of the Z20 can be approximated by just the sum of these modes is especially striking (Fig. 5d).

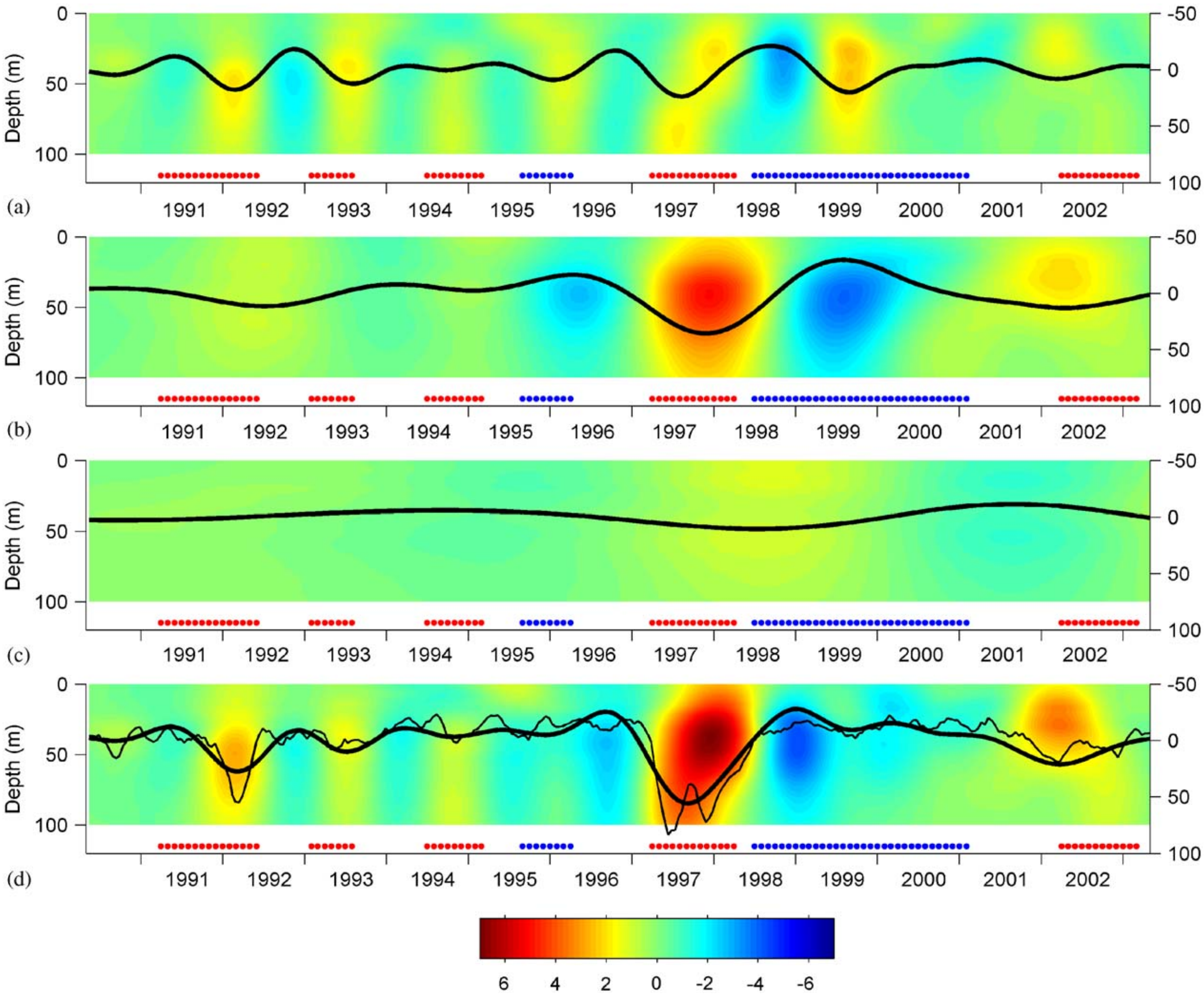

Fig. 5. Station La Libertad, details from May 1990 to May 2003, from surface (0 m) to bottom (100 m). El Niño (red dots) and La Niña (blue dots) phases are indicated according to El Niño 3.4 index. Horizontal color bar for temperature anomalies (°C) at the bottom and the right-hand side depth scale in m for the details of depth of the 20 °C isotherm anomaly (solid black line) apply. (a) Amplitude in °C of the QB mode of temperature anomalies throughout the water column and the depth of the 20 °C isotherm anomaly; (b) Amplitude in °C of the QQ mode of temperature anomalies throughout the water column and the depth of the 20 °C isotherm anomaly; (c) Amplitude in °C of the FY mode of temperature anomalies throughout the water column and the depth of the 20 °C isotherm anomaly; (d) Amplitude in °C of the sum of QB and QQ mode of temperature anomalies throughout the water column and the depth of the 20 °C isotherm anomaly, the observed anomaly of the 20 °C isotherm is shown as a thin black line.

To explore a possible change in energy distribution on the different modes when moving towards the far east, the same wavelet technique was applied to the temperature records (0–300 m) of the TAO/TRITON moorings from 165°E to 110°W across the equatorial Pacific, averaged between 2°N and 2°S. There, the QB mode explained 14.5% (165°E), 21.7% (170°W), 25.5% (140°W), and 19.7% (110°W) of the observed variance in temperature anomalies; the QQ mode accounted for 17.1% (165°E), 14.8% (170°W), 26.9% (140°W), and 43.9% (110°W) (Table 2). Hence, while moving from the western to the eastern equatorial Pacific and to the coast of

Table 2
Wavelet analysis: TAO/TRITON moorings

Detail	110°W		140°W		170°W		165°E	
	Period (years)	Variance (%)	Period (years)	Variance (%)	Period (years)	Variance (%)	Period (years)	Variance (%)
A7		4.1		7.9		8.0		7.5
D7	6.6	5.0	6.3	5.7	6.3	20.6	6.2	23.7
D6	4.6 [2.5,6.8]	43.9	4.8 [2.7,7.0]	26.9	4.9 [2.2,7.6]	14.8	4.1 [2.3,5.8]	17.1
D5	2.3 [1.5,3.1]	19.7	2.4 [1.6,3.1]	25.5	2.6 [2.0,3.1]	21.7	2.1 [1.6,2.5]	14.5
D4	1.3	11.0	1.2	13.3	1.1	8.3	1.3	19.5
D3	0.7	6.9	0.5	7.4	0.5	5.4	0.6	7.8
D2	0.3	4.8	0.2	6.3	0.2	5.1	0.2	5.6
D1	<0.2	4.7	<0.2	7.1	<0.2	6.1	<0.2	4.3

For each detail, the central period of its frequency band and the variance explained by each detail are listed. For Detail 5 and Detail 6 the upper and lower limits of the frequency band are also given in brackets. Depth-averaged temperature anomalies (0–300 m) at 110°W, 140°W, 170°W, and 165°E. The central period, associated with the largest amplitude, and the band width, defined by half amplitude method, was referred from a harmonic analysis of each detail obtained.

Ecuador, the variance explained by the QQ mode increased from about 16% to 50%, whereas the contribution of the QB mode was almost constant (between 20% and 25%), with the exception of TAO/TRITON moorings at 165°E, where it only accounted for 15%. On the other hand, the contribution of the sum of the longer periods (Detail 7 plus the approximation) decreased from 31% to about 9% when moving in the same direction, similar to the sum of the higher frequencies (Details 1–4), which decreased from 37% to 20%.

4. Eastward propagation of water column temperature anomalies (heat content)

The total temperature increase of the entire water column at station La Libertad (January–July 1997) corresponds to a 6-month long heat flux of 200 $\mathrm{W\,m^{-2}}$. Thus, the heat content of the water column, including the thermocline, is extremely important for the characterization of the oceanic impact of El Niño and the prediction of its arrival at the Ecuadorian coast.

SST is usually used to monitor the evolution and eastward propagation of temperature anomalies along the equatorial Pacific (e.g. Delcroix, 1993). Cross correlations of SST anomalies between station La Libertad and the TAO/TRITON moorings (Fig. 6a) showed an eastward propagation. The maximum cross correlations, although close to the 95% significance level for 110°W, were low (R around 0.5 for 140°W; R around 0.625 for 110°W) and spread out over a wide range of time lags (15–25 weeks for 140°W; 0–20 weeks for 110°W), making it difficult to establish a time-lagged correlation for forecast purposes. The same was true for cross correlations between SST anomalies at La Libertad and El Niño 3.4 (R around 0.4, with time lags of 20–24 weeks) and El Niño 3 (R around 0.54, with time lags of 15–20 weeks) indices (El Niño indices Trenberth, 1997) (Fig. 6b), which were both below the 95% significance level. Cross correlations between depth-averaged temperature anomalies (0–100 m) and El Niño indices produced high correlations ($R = 0.88$ and $R = 0.79$, respectively, for the Niño 3 and Niño 3.4 index) (Fig. 6c), which were, however, in phase and failed to predict the arrival of warm events in the water column off Ecuador.

When representing the temporal evolution of depth-averaged temperatures between 0 and 300 m [300 m was chosen following the computation of upper ocean heat content by Hasegawa and Hanawa (2003b); 300 m corresponds to about the maximum depth to which surface mixing extends in the tropical and sub-tropical Pacific (Ladd and Thompson, 2000)] in the TAO/TRITON moorings and depth averages between 0 and 100 m at La

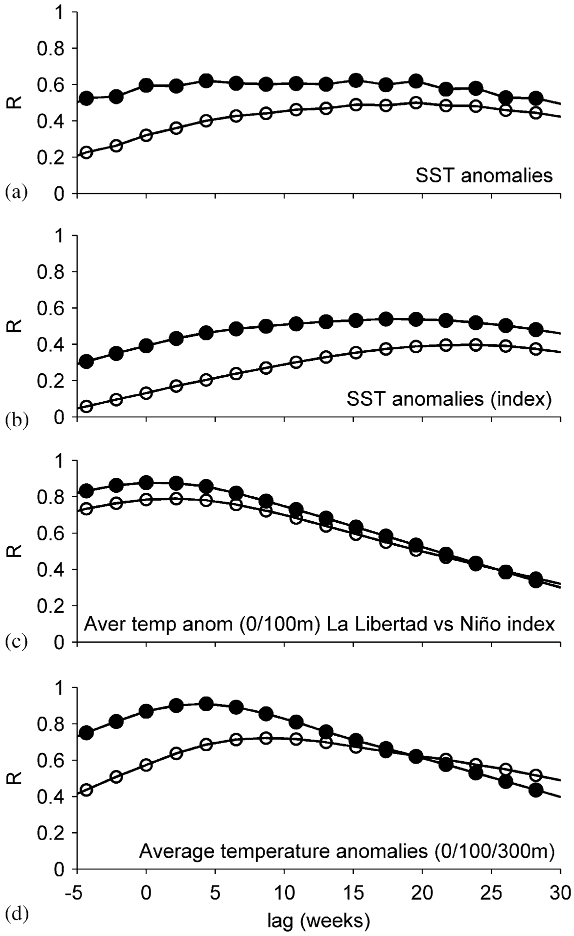

Fig. 6. Cross correlations (a) of SST anomalies between station La Libertad and 110°W (solid circle), 140°W (open circle); (b) between SST anomalies of station La Libertad and El Niño index 3 (solid circle), and El Niño index 3.4 (open circle); (c) of depth-averaged temperature anomalies at station La Libertad and El Niño index 3 (solid circle), and El Niño index 3.4 (open circle); (d) of depth-averaged temperature anomalies between station La Libertad and 110°W (solid circle), 140°W (open circle). In panels (a) and (d), TAO/TRITON moorings lead La Libertad station; in panel (b), El Niño indices lead La Libertad; in panel (c), El Niño indices and station La Libertad are in phase.

Libertad, however, an eastward propagation could be seen during recent El Niño episodes from the central equatorial Pacific to the coast of Ecuador. This was especially true for the depth-averaged temperature anomalies (Figs. 7a and b). Cross correlations of depth-averaged (0–100 m) temperature anomalies between La Libertad and depth-averaged (0–300 m) temperature anomalies of the TAO/TRITON moorings (Fig. 6d) were largest at 110°W ($R = 0.91$; time lag ~4 weeks), followed by 140°W ($R = 0.72$; time lag ~8–9 weeks), and then a low non-significant correlation at 170°W ($R = 0.43$; time lag = 30 weeks). Depth-averaged temperature anomalies appeared at the western moorings (140°W) some 8–9 weeks before reaching the Ecuadorian coast, corresponding to a propagation of about 1.25 m s^{-1}.

The above wavelet decomposition, extending from station La Libertad to the TAO/TRITON moorings up to 165°E, averaged between 2°N and 2°S. The propagation of the sum of the QB and QQ modes is shown in Fig. 7c in the form of a longitude-time plot. The average time lag between the appearance of depth-averaged temperature anomalies at 140°W and station La Libertad was estimated to range from 8–11 weeks by means of cross correlation analysis (figure not shown), corresponding to a propagation of 1.25–1.00 m s^{-1}, very close to the results obtained from the original time series of temperature anomalies, which supports a major contribution by the QB and QQ modes in the eastward movement.

5. Discussion and conclusions

We have shown that, during the 1991/1992, 1997/1998, and 2002/2003 El Niño events, temperature anomalies off Ecuador arrived much earlier in the thermocline than at the sea surface and that the amplitudes in the thermocline doubled the SST anomalies. Similarly, Hasegawa and Hanawa (2003b) showed that anomaly fields of upper-ocean heat content (OHC 0–300 m) spatially averaged over the entire equatorial Pacific, from 4°N to 4°S, led the Niño 3 index by two seasons (i.e. 6 months). Interestingly, an analysis of temperature time series from the TAO/TRITON buoys at 110°W from 1986–1998 by Harrison and Vecchi (2001) did not show a time lag between thermocline and SST anomalies. Although both time series are from the eastern equatorial Pacific, these differences suggest the

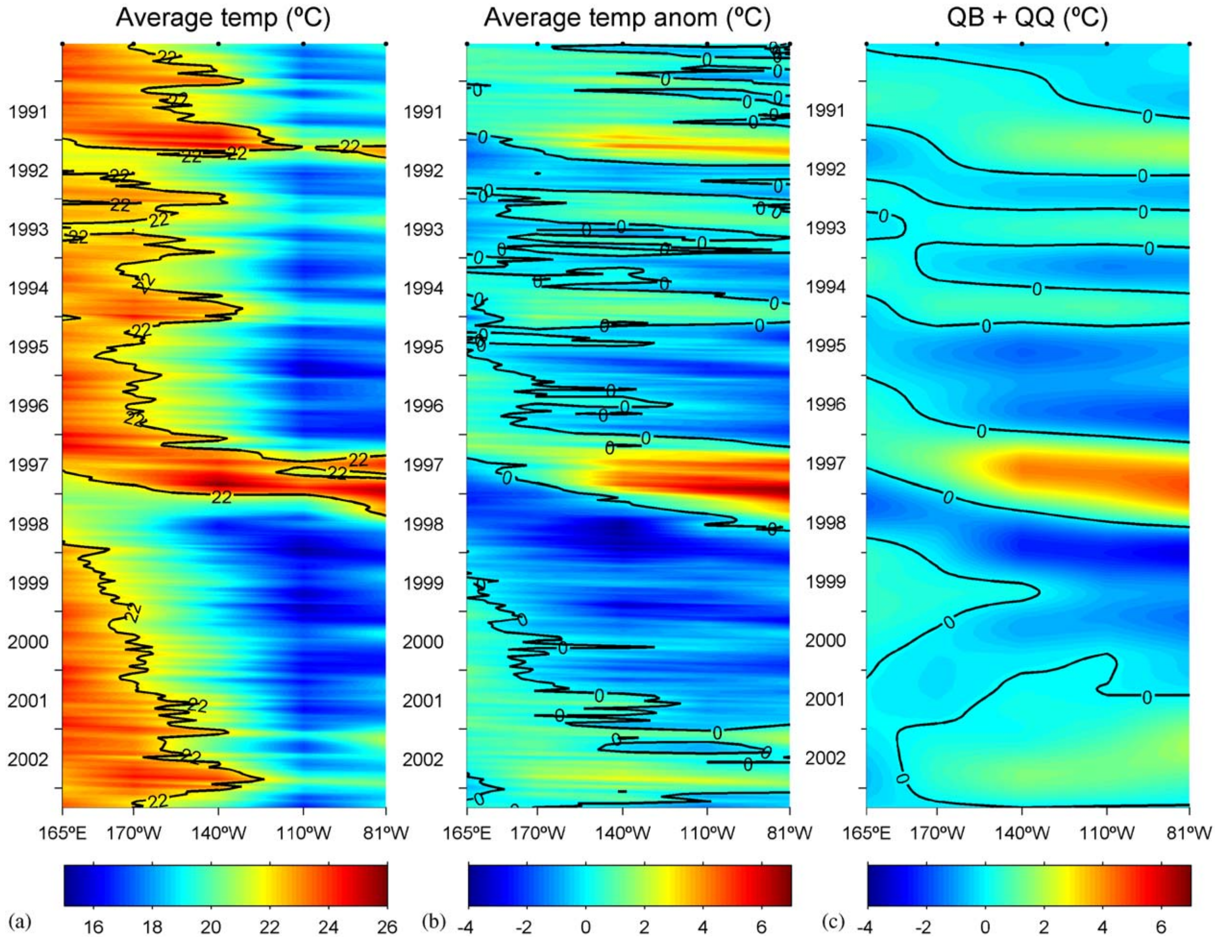

Fig. 7. Eastward propagation of depth-averaged temperatures and their anomalies. Longitude-Time plot of (a) Depth-averaged temperature; (b) Depth-averaged temperature anomalies; (c) Sum of QB and QQ from the TAO/TRITON moorings at 165°E, 170°W, 140°W, 110°W (all averaged between 2°N and 2°S and 0–300 m) and station La Libertad (0–100 m) from May 1990 to May 2003. Units are in °C, the color bars displayed below each panel apply. The black solid line in (a) represents the 22 °C isotherm and in (b) and (c), the 0 °C isotherm of the temperature anomalies.

presence of other processes such as wave reflections, modal dispersion, and tropical instability waves, which will need further investigation.

We have also shown, by means of the close relationship between mean sea level and the heat content in La Libertad, that low frequencies beyond the spectral band of inter-annual frequencies may contribute only a small percentage of the explained variance. Inter-annual variability, mainly associated with the QB and QQ modes, therefore, explains most of the observed variance.

Roughly 70% (78% when taking into account a FY oscillation mode) of the variance of the temperature anomalies in La Libertad's record can be explained by the sum of a QQ and QB mode. Similar results were obtained for depth-averaged temperatures at the TAO/TRITON moorings in the central-eastern equatorial Pacific.

These results confirm the importance of QB (D5) and QQ (D6) modes and to a lesser extend of the 5–6 year oscillation (D7), in the dynamics of the equatorial Pacific, as previously shown by various authors (e.g. White et al., 2003). Therefore, the inter-annual modes found, could have a physical explanation by means of conceptual ENSO models. Thus the western Pacific oscillator model of Weisberg and Wang (1997) for El Niño dynamics results in model oscillations with periods of 4.1–4.2 years. The recharge-discharge oscillator model for ENSO, which was put forward by Jin (1997), oscillates in periods in the range of 3–5 years. The standard case of the advective-reflective conceptual model for the oscillatory nature of ENSO by Picaut et al. (1997) performs regular lopsided oscillations with a period of about 4 years. In all cases, the QQ oscillations result from the travel speed of a combination of Kelvin and Rossby waves responsible for the ENSO cycle. Tropospheric biennial oscillations associated with El Niño are also well known. For instance, Lau and Shen (1988) detected a QB mode in global rainfall pattern associated with El Niño. Yasunari and Seki (1992) and Shen and Lau (1995) related this biennial tendency to monsoon-ENSO interaction. Later, Kim and Lau (2001) used a modified intermediate coupled model to elucidate the fundamental dynamics of biennial variability in monsoon–ENSO interactions. Depending on the strength of the monsoon–ENSO interaction, their model either oscillated with periods of 3–4 years or in QB periods. The above model results are idealized solutions, and indeed observed ENSO variability is not purely periodic. Most of the observed El Niño–La Niña cycles fall into periods captured by detail D6, or in other words can be described as presenting QQ periods.

Irregular inter-annual variability might result from the coupling of the atmosphere and ocean (Munnich et al., 1991). Mantua and Battisti (1994) analyzed the Zebiak/Cane numerical model and demonstrated that irregularities in the ENSO cycle were owing to the interaction between two coupled unstable atmosphere/ocean modes. Further, various investigators have proposed that disturbances propagating into the tropical Pacific from the extratropics or the Indian Ocean can trigger or modify the ENSO cycle (see, e.g. Barnett et al., 1989). Hence, energy found in the QB and 5–6 year periods might as well be, at least partly, owing to fluctuations around the typical El Niño–La Niña periods. In contrast, the coincidence of diverse mechanisms may give rise to particular El Niño events, as different periods enhance their individual dynamics when concurring in phase, as appears to be the case in the far eastern equatorial Pacific for the 1991/1992 (QB + QQ) and 1997/1998 (QB + QQ + FY) El Niño events.

Incidentally, the QQ mode appears to gain importance when moving from the western-central equatorial Pacific to the far east, whereas the contribution of the QB mode is almost constant. The change of energy distribution on the modes, when propagating eastward, indicates a probable non-linear mechanism at work. This can be related to modal dispersion processes that couple different baroclinic modes (Busalacchi and Cane, 1988).

Although not unexpected, given the already existent knowledge derived from TAO/TRITON moorings, we have re-confirmed the importance of the water column's heat content (e.g. McPhaden, 1999; McPhaden and Yu, 1999; Meinen and McPhaden, 2000), including the thermocline, in characterizing El Niño's oceanic impact and predicting its arrival at the Ecuadorian coasts. Our results show that heat content anomalies, expressed in depth-averaged temperature anomalies, appear an average of 8–9 weeks earlier at 140°W than at the Ecuadorian coast, 6550 km away. Thus, using the depth-averaged temperature anomalies at the TAO/TRITON 140°W station as an additional and complementary index of El Niño's impact on the water column's thermal structure, and particularly for predicting El Niño's arrival in the sub-surface waters off the equatorial coast of Ecuador, seems reasonable. This is most practical and useful given that El Niño's impact is most relevant to a regime shift in marine ecosystems and has vital socio-economic consequences.

Most forecasts concentrate on the prediction of SST anomalies along the equatorial Pacific, which, of course, includes the oceanic region off Ecuador. Forecasts are based on coupled atmosphere/ocean numerical models where the atmospheric component might be a dynamic or statistical model (e. g. Dewitte et al., 2003). The skill of the numerous models varies from model to model and for different El Niño events. Our analysis, plus those of other authors, indicate that warming off Ecuador, El Niño region 2, first occurs in the thermocline and later in SST. Positive anomalies observed in the thermocline off Ecuador are led by anomalous warming in the depth-averaged water column at TAO/TRITON stations at 140°W and 110°W. Temperature data (0–500 m) from these moorings are transmitted in real-time via the Argos satellite system and available at http://www.pmel.noaa.gov/tao. A reliable historic data base at 140°W, between 2°N and 2°S, extends back to 1987 and at 110°W, between 2°N and 2°S, to 1986. This information allows a near real-time computation of depth-averaged temperature anomalies, which could easily be used, complementary to model forecasts, to predict the arrival of the warming events off Ecuador at least 2 months ahead of time.

This 8–9 week time lag between the arrival of thermocline anomalies at 140°W and La Libertad corresponds to a propagation of $1.25\,\mathrm{m\,s^{-1}}$, which is in between the speed of the second and third baroclinic vertical Kelvin wave mode (Table 1; Kessler and McPhaden, 1995). Further analysis of phase propagation during El Niño events only, however, reveals variable propagation speeds between 1.66 and $1.00\,\mathrm{m\,s^{-1}}$ for 1991/1992 and 1997/1998, respectively, which does not contradict the eastward propagation of heat content along the Equator, but points to the possible participation of higher order Kelvin modes in ENSO dynamics at the far eastern boundaries. Further, extending the wavelet decomposition to the TAO/TRITON moorings shows that the sum of QB and QQ oscillations between 140°W and La Libertad accounts for most of the propagation observed in the temperature anomalies in the eastern equatorial Pacific.

Processes in the far eastern equatorial Pacific are very complex, e.g. including wave reflection, nonlinear processes, modal dispersion (Dewitte et al., 1999). Regional data are needed in order to study these processes. We are confident that the advent of this new time series (or others that may be provided by INOCAR over the equatorial areas), complementing TAO/TRITON, may assist in the future to help understand some peculiarities of ENSO dynamics.

Acknowledgments

The authors would like to thank B. Dewitte, A. Forbes, and three anonymous reviewers for helpful comments on an earlier version of this manuscript. This work was supported by the DAAD (cod. A/99/14453) and MECESUP/UCO-0002 scholarship program, Chilean National Research Council (FONDAP-COPAS, Project No 15010007), and INOCAR. Temperature data at moorings along the equator were obtained from the TAO/TRITON Project Office.

Appendix A

A.1. Wavelet multi-resolution analysis

Wavelets or "small waves" are oscillatory functions with zero mean. Daubechies's wavelets, which are in use in this study, in addition are functions with compact support. Wavelets are orthonormal functions obtained by shifting and stretching a mother wavelet, $\psi(t)$. The wavelet transform of a discrete signal is known as the DWT and is related to the wavelet coefficients $C(a,b)$ defined as the inner product of the signal and the translated and dilated mother wavelet:

$$\mathrm{C}(a,b) = \left\langle s(t), \quad \frac{1}{\sqrt{a}}\,\psi\left(\frac{t-b}{a}\right)\right\rangle,$$
$$a = 2^j, \quad b = k2^j, \quad (j,k) \in Z.$$

From an intuitive point of view, the wavelet transform (WT) of a signal, $s(t)$, where t is time, is a two-dimensional sequence, $C(a,b)$, where a achieves a dilation (shrink and stretch) of the mother wavelet, ψ, and b determines its translation (shift). The dilation takes values of the form $a = 2^j$ where j is an integer. At any dilation 2^j, the translation parameter takes values of the form $k2^j$, where k again is an integer. The values $C(a,b)$ are related to values of the wavelet transform $\mathrm{WT}[s(t)]$ at $a = 2^j$ and $b = k2^j$. This process is called dyadic sampling because consecutive values of the discrete scales as well the corresponding sampling intervals differ by a factor of two. The scaled wavelet is compared to the original signal by means of variations of its position, to obtain the wavelet coefficients $C(a,b)$. A high value of $C(a,b)$ corresponds to a great similarity between the wavelet (scaled and shifted) and the corresponding portion of the signal.

Among one of the main applications of DWT is the wavelet multi-resolution analysis. By forming a series of half-band filters that divide a spectrum into a high-frequency and a low-frequency band, the original signal is decomposed into a hierarchical set of j approximations (low frequencies) and j details (high-frequencies).

As an example let us consider an original time series and call it approximation at level 0, denoted by $A0$. In the orthogonal discrete wavelet decomposition procedure, the generic step splits the approximation into two parts; a vector of approximation coefficients (A) and a vector of detail coefficients (D). At each level j, the j-level time series A_j, or approximation at level j, and the j-level time series D_j, or detail at level j are built. D_j reads

$$D_j(t) = \sum_{k \in Z} C(j,k)\psi_{j,k}(t).$$

Suppose that we choose 3 levels for the decomposition: $A0 = A1 + D1$, and since $A1 = A2 + D2$, and $A2 = A3 + D3$, it implies that $A0 = A3 + D3 + D2 + D1$. Time series $A0$ is, therefore, the sum of the approximation $A3$ and intermediate details $D1$, $D2$ and $D3$. Within the approximation $A3$ are contained all the lowest frequencies that are not captured within the band passed time series $D1$, $D2$ and $D3$, respectively going from high to low frequencies. Details at different decomposition levels are orthogonal to each other. In general, at reference level J of the decomposition the approximation at level J is computed by

$$A_J = \sum_{j>J} D_j$$

and the original time series, s, can be completely reconstructed applying

$$s = A_J + \sum_{j \leqslant J} D_j.$$

References

Barber, R.T., Chavez, F.P., 1983. Biological consequences of El Niño. Science 222, 1203–1210.

Barnett, T.P., Dumenil, L., Schlese, U., Roeckner, E., Latif, M., 1989. The effect of Eurasian snow cover on regional and global climate variations. Journal of the Atmospheric Sciences 46, 661–685.

Boulanger, J.-P., Fu, L.-L., 1996. Evidence of boundary reflection of Kelvin and first-mode Rossby waves from TOPEX/POSEIDON sea level data. Journal of Geophysical Research 101, 16361–16371.

Brassington, G.B., 1997. The modal evolution of the southern oscillation. Journal of Climate 10, 1021–1034.

Busalacchi, A.J., Cane, M.A., 1988. The effect of varying stratification on low-frequency equatorial motions. Journal of Physical Oceanography 18, 801–812.

Cane, M.A., 1983. Oceanographic events during El Niño. Science 222, 1189–1195.

Cucalón, E., 1987. Oceanographic variability off Ecuador associated with an El Niño event in 1982–1983. Journal of Geophysical Research 92, 14309–14322.

Daubechies, I., 1992. Ten Lectures on Wavelets. CBMS-NSF Regional Conference Series in Applied Mathematics, No. 61. Society for Industrial and Applied Mathematics, Philadelphia 357pp.

Delcroix, T., 1993. Seasonal and interannual variability of sea surface temperatures in the Tropical Pacific, 1969–1991. Deep-Sea Research Part I 40, 2217–2228.

Dewitte, B., Reverdin, G., Maes, C., 1999. Vertical structure of an OGCM simulation of the equatorial Pacific Ocean in 1985–94. Journal of Physical Oceanography 29, 1542–1570.

Dewitte, B., Gushchina, D., duPenhoat, Y., Abarca del Rio, R., 2003. SST predictions with an intermediate coupled model of the tropical Pacific. WWW page http://grads.iges.org/ellfb/Jun03/dewitte/dewitte.htm

Harrison, D.E., Vecchi, G.A., 2001. El Niño and La Niña-Equatorial Pacific thermocline depth and sea surface temperature anomalies, 1986–98. Geophysical Research Letters 28, 1051–1054.

Hasegawa, T., Hanawa, K., 2003a. Decadal-scale variability of upper ocean heat content in the tropical Pacific. Geophysical Research Letters 30.

Hasegawa, T., Hanawa, K., 2003b. Heat content variability related to ENSO events in the Pacific. Journal of Physical Oceanography 33, 407–421.

Jiang, N., Neelin, J.D., Ghil, M., 1995. Quasi-quadrennial and quasi-biennial variability in the equatorial Pacific. Climate Dynamics 12, 101–112.

Jin, F.F., 1997. An equatorial ocean recharge paradigm for ENSO. 1. Conceptual model. Journal of the Atmospheric Sciences 54, 811–829.

Kessler, W.S., McPhaden, M.J., 1995. Oceanic Equatorial Waves and the 1991–93 El Niño. Journal of Climate 8, 1757–1774.

Kim, K.M., Lau, K.M., 2001. Dynamics of monsoon-induced biennial variability in ENSO. Geophysical Research Letters 28, 315–318.

Köberle, C., Philander, S.G.H., 1994. On the processes that control seasonal-variations of sea-surface temperatures in the Tropical Pacific-Ocean. Tellus Series a-Dynamic Meteorology and Oceanography 46, 481–496.

Kumar, P., Foufoula-Georgiou, E., 1997. Wavelet analysis for geophysical applications. Reviews of Geophysics 53, 385–412.

Ladd, C., Thompson, L., 2000. Formation mechanisms for North Pacific central and eastern subtropical mode waters. Journal of Physical Oceanography 30, 868–887.

Lau, K.M., Shen, S.H., 1988. On the dynamics of intraseasonal oscillations and ENSO. Journal of the Atmospheric Sciences 45, 1781–1797.

Mallat, S.G., 1998. A Wavelet Tour of Signal Processing. Academic Press, San Diego 577pp.

Mantua, N.J., Battisti, D.S., 1994. Evidence for the delayed oscillator mechanism for ENSO: the "Observed" Oceanic Kelvin Mode in the Far Western Pacific. Journal of Physical Oceanography 24, 691–699.

McPhaden, M.J., 1999. Genesis and evolution of the 1997–98 El Niño. Science 283, 950–954.

McPhaden, M.J., Yu, X., 1999. Equatorial waves and the 1997–98 El Niño. Geophysical Research Letters 26, 2961–2964.

McPhaden, M.J., Busalacchi, A.J., Cheney, R., Donguy, J.R., Gage, K.S., Halpern, D., Ji, M., Julian, P., Meyers, G., Mitchum, G.T., Niiler, P.P., Picaut, J., Reynolds, R.W., Smith, N., Takeuchi, K., 1998. The tropical ocean global atmosphere observing system: a decade of progress. Journal of Geophysical Research 103, 14169–14240.

Meinen, C.S., McPhaden, M.J., 2000. Observations of warm water volume changes in the equatorial Pacific and their relationship to El Niño and La Niña. Journal of Climate 13, 3551–3559.

Munnich, M., Cane, M.A., Zebiak, S.E., 1991. A study of self-excited oscillations of the Tropical Ocean atmosphere system. 2. Nonlinear cases. Journal of the Atmospheric Sciences 48, 1238–1248.

Percival, D.B., Mofjeld, H.O., 1997. Analysis of subtidal coastal sea level fluctuations using wavelets. Journal of the American Statistical Association 92, 868–880.

Picaut, J., Masia, F., duPenhoat, Y., 1997. An advective-reflective conceptual model for the oscillatory nature of the ENSO. Science 277, 663–666.

Rasmusson, E.M., Wallace, J.M., 1983. Meteorological aspects of the El Niño Southern oscillation. Science 222, 1195–1202.

Shen, S.H., Lau, K.M., 1995. Biennial oscillation associated with the East-Asian summer monsoon and tropical sea-surface temperatures. Journal of the Meteorological Society of Japan 73, 105–124.

Trenberth, K.E., 1997. The definition of El Niño. Bulletin of the American Meteorological Society 78, 2771–2777.

Weisberg, R.H., Wang, C.Z., 1997. A western Pacific oscillator paradigm for the El Niño Southern oscillation. Geophysical Research Letters 24, 779–782.

White, W.B., Tourre, Y.M., Barlow, M., Dettinger, M., 2003. A delayed action oscillator shared by biennial, interannual, and decadal signals in the Pacific Basin. Journal of Geophysical Research 108.

Yasunari, T., Seki, Y., 1992. Role of the Asian monsoon on the interannual variability of the global climate system. Journal of the Meteorological Society of Japan 70, 177–189.

Zhang, X., Sheng, J., Shabbar, A., 1998. Modes of interannual and interdecadal variability of Pacific SST. Journal of Climate 11, 2556–2569.